

Joint Summarization of Large-scale Collections of Web Images and Videos for Storyline Reconstruction

Gunhee Kim
Disney Research Pittsburgh
gunhee@cs.cmu.edu

Leonid Sigal
Disney Research Pittsburgh
lsigal@disneyresearch.com

Eric P. Xing
Carnegie Mellon University
epxing@cs.cmu.edu

Abstract

In this paper, we address the problem of jointly summarizing large sets of Flickr images and YouTube videos. Starting from the intuition that the characteristics of the two media types are different yet complementary, we develop a fast and easily-parallelizable approach for creating not only high-quality video summaries but also novel structural summaries of online images as storyline graphs. The storyline graphs can illustrate various events or activities associated with the topic in a form of a branching network. The video summarization is achieved by diversity ranking on the similarity graphs between images and video frames. The reconstruction of storyline graphs is formulated as the inference of sparse time-varying directed graphs from a set of photo streams with assistance of videos. For evaluation, we collect the datasets of 20 outdoor activities, consisting of 2.7M Flickr images and 16K YouTube videos. Due to the large-scale nature of our problem, we evaluate our algorithm via crowdsourcing using Amazon Mechanical Turk. In our experiments, we demonstrate that the proposed joint summarization approach outperforms other baselines and our own methods using videos or images only.

1. Introduction

The recent explosive growth of online multimedia data has posed a new set of challenges in computer vision research. One of such infamous difficulties is that much of the data accessible to users are neither refined nor structured for later use, and subsequently has led to the *information overload* problem; users are often overwhelmed by the flood of unstructured pictures and videos. Therefore, it is increasingly important to automatically summarize a large set of multimedia data in an efficient yet comprehensive way.

In this paper, we address the problem of joint summarization of large sets of online images (*e.g.* Flickr) and videos (*e.g.* YouTube), particularly in terms of *storylines*. Handling both still images and videos is becoming necessary, due to the recent convergence between cameras and

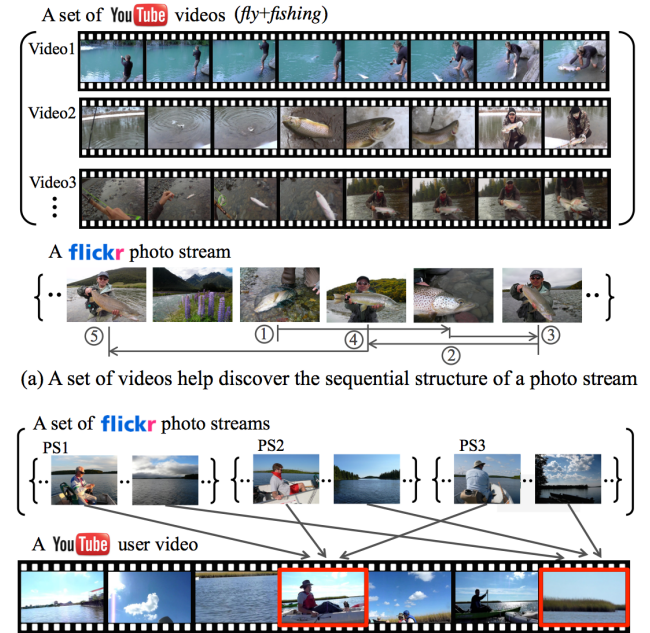


Figure 1. Benefits of jointly summarizing Flickr images and YouTube videos illustrated on a *fly+fishing* activity. (a) Although images in a photo stream are taken consecutively, the underlying sequential structure between images is missing, which can be discovered with the help of a collection of videos. (b) Typical user videos contain noisy and redundant information, which can be removed using similarity votes cast by a large set of images that are taken more carefully from canonical viewpoints. The frames within red boxes are selected as video summary using our method.

camcorders. For example, any smartphone user can seamlessly record the memorable moments via both photos and videos by switching between the two modes with a tap.

More importantly, jointly summarizing images and videos is *mutually-rewarding* for the summarization purpose, because their characteristics as recording media are different yet complementary (See Fig. 1). The strength of images over videos lies in that images are more carefully taken so that they capture the subjects from canonical viewpoints in a more semantically meaningful way. However,

still images are fragmentally recorded, and thus the sequential structure is often missing even between consecutive images in a single photo stream. On the other hand, videos are *motion pictures*, which convey temporal smoothness between frames. However, one major issue with videos is that they contain redundant and/or noisy information with, often, poor quality, such as backlit subjects, motion blurs, overexposure, and full of trivial backgrounds like sky or water. Therefore, as shown in Fig. 1, we take advantage of sets of images to get rid of such noisy, redundant, or semantically meaningless parts of videos. In the reverse direction, we leverage sets of videos to glue fragmented images into coherent and smooth threads of storylines.

We first collect large sets of photo streams from Flickr and user videos from YouTube for a topic of interest (*e.g.* *fly+fishing*). We summarize each video with a small set of keyframes using similarity votes cast by the images from the most similar photo streams. Subsequently, leveraging the continuity information between the selected keyframes in videos, we discover the underlying sequential structure between images in each photo stream, and summarize the sets of photo streams in the form of *storyline graphs*. We represent the storylines as directed graphs in which the vertices correspond to dominant image clusters, and the edges connect the vertices that sequentially recur in many photo streams and videos. The summarization in the form of storyline graphs is advantageous especially for the topics that consist of a sequence of activities or events repeated across the photo and video sets, such as recreational activities, holidays, and sports events. Moreover, the storyline graphs can characterize various branching narrative structures associated with the topic, which help users understand the underlying big picture surrounding the topic (*e.g.* activities that people usually enjoy during their *fly+fishing* trips).

In our approach, the video summarization is achieved by diversity ranking on the similarity graphs between images and video frames (section 3). The reconstruction of storyline graphs is formulated as the inference of sparse time-varying directed graphs from a set of directed trees created from photo streams with assistance of videos (section 4). As a result, our method provides several appealing properties, especially for large-scale problems, such as optimality guarantee, linear complexity, and easy parallelization.

For evaluation, we collect the datasets of 20 outdoor recreational activities, which consist of about 2.7M images of 35K photo streams from Flickr and 16K videos from YouTube. Due to the large-scale nature of our problems, we evaluate our algorithms via crowdsourcing using Amazon Mechanical Turk (section 5). In our experiments, we quantitatively show that the proposed joint summarization approach outperforms other baselines and our method using videos or images only, for the both tasks of video summarization and storyline reconstruction.

1.1. Previous work

Here we overview representative literature from three lines of research that are related to our work.

Structured image summarization. One of most traditional ways to summarize image databases is the *image retrieval* that returns a small number of representative images with ranking scores for a given topic (*e.g.* Google/Bing image search engines). Recently, there have been several important threads of image summarization work in computer vision as follows. The first notable direction is to organize image databases with structural visual concepts such as WordNet hierarchy [5] or word dictionaries [21]. Another line of work is to organize visitors' unstructured community photos of popular landmarks in a spatially browsable way [18]. However, the concept of stories has not been explored much for structured image summarization yet. The work of [9] is related to our work in that it leverages Flickr images and its objective is motivated by the photo storyline reconstruction. However, [9] is a preliminary research that solely focuses on alignment and segmentation of photo streams; no storyline reconstruction is explored.

Story-based video summarization. The story-based video summary has been actively studied in the context of sports [7] and news [15]. However, in such applications, the videos of interest usually contain a small number of specified actors in fixed scenes with synchronized voices and captions, all of which are not available in unstructured user images and videos on the Web. The work of [8] may be one of the closest to our work, because images are used as a prior to create semantically-meaningful summaries of user-generated videos on eBay sites. The key difference of our work is that we complete a loop between jointly summarizing images and videos in a mutually-rewarding way. Also, our storyline summaries can support multiple branching structures unlike simple keyframe summaries of [8]. Lately, the summarization of ecocentric videos [12, 13] has emerged as an interesting topic, in which compact story-based summaries are produced from user-centric daylife videos. The objective of our work differs in that we are interested in the collections of online images and videos that are independently taken by multiple anonymous users, instead of a single user's hours-long videos.

Computer vision leveraging both images and videos. Recently, it is gaining popularity to address challenging computer vision problems by leveraging both images and videos. New powerful algorithms have been developed by pursuing synergic interplay between the two complementary domains of information, especially in the areas of adapting object detectors between images and videos [16, 20], human activity recognition [3], and event detection [4]. However, the storyline reconstruction extracted from both images and videos still remains as a novel and largely under-addressed problem.

1.2. Summary of Contributions

We summarize the contributions of this work as follows.

(1) We propose an approach to jointly summarize large sets of online images and videos in a mutually-rewarding way. Our method creates not only high-quality video summary but also a novel structural summary of online images as *storyline graphs*, which can visualize various events and activities associated with the topic in a form of branching networks. To the best of our knowledge, our work is the first attempt so far to leverage both online images and videos for building of storyline graphs.

(2) We develop algorithms for video summarization and storyline reconstruction, properly addressing several key challenges of related large-scale problems, including optimality guarantees, linear complexity, and easy parallelization. With experiments on large-scale Flickr and YouTube datasets and crowdsourcing evaluations through Amazon Mechanical Turk, we show the superiority of our approach over competing methods for both summarization tasks.

2. Problem Setting

Input. The input is a set of photo streams $\mathcal{P} = \{P^1, \dots, P^L\}$ and a set of videos $\mathcal{V} = \{V^1, \dots, V^N\}$, for a topic class of interest. L and N indicate the number of input photo streams and videos, respectively. Each photo stream, denoted by $P^l = \{p_1^l, \dots, p_{L^l}^l\}$, is a set of photos taken in sequence by a single photographer within a fixed period of time $[0, T]$, single day in this paper. We assume that each image p_i^l is associated with a timestamp t_i^l , and images in each photo stream are temporally ordered. We uniformly sample each video into a set of frames every 0.5 sec, which is denoted by $V^n = \{v_1^n, \dots, v_{N^n}^n\}$. As a notational convention, we use superscripts to denote photo streams/videos and subscripts to denote images/frames.

Output. The output of our algorithm is two-fold. The first output is the summary S^n of each video $V^n \in \mathcal{V}$ (*i.e.* $S^n \subset V^n$). We pursue keyframe-based summarization (*e.g.* [8]), in which S^n is chosen as ν^n number of most representative but discriminative keyframes out of V^n . Its technical details will be discussed in Section 3. The second output is the storyline graphs $\mathcal{G} = (\mathcal{O}, \mathcal{E})$. The vertices \mathcal{O} correspond to dominant image clusters across the dataset, and the edge set \mathcal{E} connects the vertices that sequentially recur in many photo streams and videos. More rigorous mathematical definition will be given in Section 4.

Image Description and Similarity Measure. We apply three different feature extraction methods to images and frames of videos. We densely extract HSV color SIFT and histogram of oriented edge (HOG) feature on a regular grid of each image and frame at steps of 4 and 8 pixels, respectively. We build an L_1 -normalized three-level spatial pyramid histogram for each feature type. Finally, we obtain the *Tiny* image feature [21], which is RGB values of a 32×32

resized image. For similarity measure σ , we use histogram intersection. The three descriptors are equally weighted.

K-NN graphs between photo streams and videos. Due to the extreme diversity of the Web images and videos associated even with the same keyword, we build K -nearest graphs between \mathcal{P} and \mathcal{V} so that only sufficiently similar photo streams and videos help summarize one another.

For each photo stream $P^l \in \mathcal{P}$, we find K_P -nearest videos calculating the similarity by Naive-Bayes Nearest-Neighbor method [2] as follows. For all pairs of photo stream P^l and videos $V^n \in \mathcal{V}$, we obtain the first nearest neighbor in V^n of each image $p \in P^l$, denoted by $\text{NN}(p)$. The similarity from P^l to V^n is computed by $\sum_{p \in P^l} \|\sigma(p, \text{NN}(p))\|^2$. As results, we can find $\mathcal{N}(P^l)$ as the K_P -nearest videos to P^l . We set $K_p = c \cdot \log(|\mathcal{V}|)$ with $c = 1$. Likewise, we run the same procedure to obtain K_V -nearest photo streams $\mathcal{N}(V^n)$ for each video V^n .

Since we leverage sufficiently large image/video datasets that reasonably well cover each topic, we observe that the *domain difference* between images and videos does not affect performance much. For example, when we find out K nearest images to a video frame from our image dataset, the matched frame and images tend to be similar to one another.

3. Video Summarization

The summarization of each video $V^n \in \mathcal{V}$ runs as follows. We first build a similarity graph $\mathcal{G}_V^n = (\mathcal{X}^n, \mathcal{E}^n)$ where the node set is the frames in V^n and the images of its neighbor photo streams $\mathcal{N}(V^n)$ (*i.e.* $\mathcal{X}^n = V^n \cup \mathcal{N}(V^n)$), and the edge set consists of two groups: $\mathcal{E}^n = \mathcal{E}_I^n \cup \mathcal{E}_O^n$. \mathcal{E}_I^n is the edge set between the frames within V^n , in which consecutive frames are connected as k -th order Markov chain, and the weights are computed by feature similarity. \mathcal{E}_O^n defines the edges between frames in V^n and the images of $\mathcal{N}(V^n)$. More specifically, each image in $\mathcal{N}(V^n)$ casts similarity votes by connecting with its k_P -nearest frames with the weight of feature similarity. Since most images shared online are carefully taken by photographers who try to express their intents to be as clear as possible, even simple similarity voting by a crowd of such images can discover high-quality and semantically-meaningful keyframes, which will be demonstrated in the experiments (Section 5).

Once we build the graph $\mathcal{G}_V^n = (\mathcal{X}^n, \mathcal{E}^n)$, we select ν^n keyframes as a summary of V^n using the diversity ranking algorithm proposed in [10], which is formulated as a temperature maximization by placing ν^n number of heat sources in V^n . Intuitively, the sources should be located in the nodes that are densely connected to other nodes with high edge weights. At the same time, the sources should be sufficiently distant from one another because nearby nodes to the sources will already have high temperatures. We let \mathbf{G}^n be the adjacency matrix of \mathcal{G}_V^n . In order to model the heat dissipation, a ground node g is connected to all nodes

with a constant dissipation conductance z (*i.e.* appending an $|\mathbf{G}^n| \times 1$ column \mathbf{z} to the end of \mathbf{G}^n). The optimization of ν^n keyframe selection can be expressed by

$$\begin{aligned} \max & \sum_{x \in \mathcal{X}^n} u(x) \\ \text{s.t. } & u(x) = \frac{1}{d_x} \sum_{(x,y) \in \mathcal{E}^n} \mathbf{G}(y,x) u(y) \text{ for } d_x = \sum_{(x,y) \in \mathcal{E}^n} \mathbf{G}(y,x) \\ & u(g) = 0, \quad u(s) = 1 \text{ for } s \in S^n \subset V^n, |S^n| \leq \nu^n, \end{aligned} \quad (1)$$

where $u(x)$ is the temperature at x and d_x is the degree of x . The first constraint enforces the temperature of each node to observe the diffusion law. The second constraint sets the temperature of ground and heat sources to 0 and 1, respectively. S^n is the set of ν^n selected keyframes out of V^n . In [10], the objective of Eq.(1) is proved to be *submodular*, and thus we can compute a constant factor approximate solution by a simple greedy algorithm, which starts with an empty S^n and iteratively adds the frame s that maximizes the marginal temperature gain, $\Delta U = U(S^n \cup \{s\}) - U(S^n)$, where $U(S^n) = \sum_{x \in \mathcal{X}^n} u(x)$ when sources are located in S^n . We keep increasing ν^n until the marginal temperature gain ΔU is below the threshold $\gamma = 0.01 \cdot \Delta U_1$ (*i.e.* 1% of the gain of the first selected keyframe).

4. Photo Storyline Reconstruction

In this section, we discuss the reconstruction of a storyline graph $\mathcal{G} = (\mathcal{O}, \mathcal{E})$ from a set of photo streams \mathcal{P} with assistance of the video set \mathcal{V} .

4.1. Definition of Storyline Graphs

Definition of Vertices. Since the image sets are large and ever-growing and much of images are highly overlapped, it is inefficient to build a storyline graph over individual images. Hence, the vertices \mathcal{O} are preferentially defined as *image clusters*. Since each image/frame is associated with J descriptors ($J = 3$ as in section 2), for each descriptor type j , we build D_j visual clusters ($D_j = 600$) by applying the K-means to randomly sampled images. By assigning the nearest visual cluster, each image can be represented as J vectors of $\mathbf{x}^{(j)} \in \mathbb{R}^{D_j}$ with only one nonzero indicating its cluster membership (*i.e.* identically as a single vector $\mathbf{x} \in \mathbb{R}^D$ by concatenating all J vectors)¹. Finally, each visual cluster corresponds to a vertex in \mathcal{O} (*i.e.* $|\mathcal{O}| = D = \sum_{j \in J} D_j = 1,800$ in our case).

Definition of Edges. We let the edge set $\mathcal{E} \subseteq \mathcal{O} \times \mathcal{O}$ satisfy the following two properties [11, 19]. (i) \mathcal{E} should be *sparse*. The *sparsity* is encouraged in order to avoid an unnecessarily complex narrative structure; instead we retain only a small number of strong story branches per node. (ii) \mathcal{E} should be *time-varying*; \mathcal{E} smoothly changes over time

¹ Trivially, we can extend the model by allowing soft assignment in which an image is associated with c multiple clusters with weights.

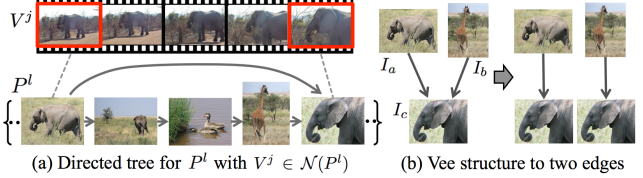


Figure 2. We build the directed tree \mathcal{T}^l for a photo stream P^l with its nearest videos $\mathcal{N}(P^l)$. (a) First, images in P^l are represented by a k -th order Markov chain ($k = 1$). Then, additional links are connected based on one-to-one correspondences between images in P^l and keyframes of $V^j \in \mathcal{N}(P^l)$. (b) Since the vee structure is an impractical artifact, it is replaced by two parallel edges.

in $t \in [0, T]$, since popular transitions between images vary over time. For example, in the *snowboarding* photo streams, the *skiing* images may be followed by *lunch* images around noon but by *sunset* images in the evening.

Based on the two requirements, we obtain a set of time-specific $\{\mathbf{A}^t\}$ for $t \in [0, T]$, where \mathbf{A}^t is the adjacency matrix of \mathcal{E}^t . Although we can compute \mathbf{A}^t at any time t , in practice, we uniformly split $[0, T]$ into multiple points (*e.g.* every 30 minutes), at which \mathbf{A}^t is estimated. In addition, we penalize nonzero elements of each \mathbf{A}^t for sparsity.

4.2. Modeling of Storyline Graphs

We formulate the inference of the storyline graph as a maximum likelihood estimation problem. Our first step is to represent each photo stream P^l as a directed tree \mathcal{T}^l , using the sequential relevance obtained from the photo stream itself and its neighbor videos. As shown in a toy example of Fig.2, we first connect the images of P^l as a k -th order Markov chain, based on that consecutive images in a photo stream are loosely sequential. Then, we perform the summarization for each neighbor video $V^j \in \mathcal{N}(P^l)$ using the algorithm in section 3. We can use a large ν^j to detect sufficiently many keyframes. Next, we find one-to-one bipartite matching between the selected frames and the images in P^l using the Hungarian algorithm. Then, we additionally connect any pairs of images in P^l that are linked by consecutive frames in V^j . We assign edge weights using the feature similarity. Finally, as shown in Fig.2.(b), we replace any *vee* structure, which is an impractical artifact, with two parallel edges by copying I_c . In our model, the *vee* structure occurs because I_a and I_b can be followed by I_c , not because both I_a and I_b must occur in order for I_c to appear.

In the current formulation, videos are used only for discovering the edges of storyline graphs, and do not contribute to the definition of vertices. This is due to our assumption that storyline graphs are structural summaries of the images. However, it is straightforward to include video frames for the node construction without modifying the algorithm.

We now derive the likelihood $f(\mathcal{P})$ of an observed set of photo streams $\mathcal{P} = \{P^1, \dots, P^L\}$. Note that each image p_i^l in P^l is associated with cluster membership vector \mathbf{x}_i^l and

timestamp t_i^l . The likelihood $f(\mathcal{P})$ is defined as follows.

$$f(\mathcal{P}) = \prod_{l=1}^L f(P^l), \text{ where } f(P^l) = \prod_{\mathbf{x}_i^l \in P^l} f(\mathbf{x}_i^l, t_i^l | \mathbf{x}_{p(i)}^l, t_{p(i)}^l) \quad (2)$$

where $\mathbf{x}_{p(i)}^l$ and denote the parent of \mathbf{x}_i^l in the directed tree \mathcal{T}^l . Since no vee structure is allowed, each image has only one parent. For the transition model $f(\mathbf{x}_i^l, t_i^l | \mathbf{x}_{p(i)}^l, t_{p(i)}^l)$, we use the *linear dynamics model*, as one of the simplest transition models for dynamic Bayesian networks (DBN):

$$\mathbf{x}_i^l = \mathbf{A}_e \mathbf{x}_{p(i)}^l + \epsilon, \text{ where } \epsilon \sim \mathcal{N}(\mathbf{0}, \sigma^2 \mathbf{I}) \quad (3)$$

where ϵ is a vector of Gaussian noise with zero mean and variance σ^2 . In order to model time difference between $t_{p(i)}^l$ and t_i^l , we use the *exponential* rate function that is widely used for the temporal dynamics of diffusion networks [17]: the (x, y) element a_{xy} of \mathbf{A}_e has the form of $\alpha_{xy} \exp(-\alpha_{xy} \Delta_i)$ where $\Delta_i = |t_i^l - t_{p(i)}^l|$ and α_{xy} is the transmission rate from visual cluster x to y . As $\alpha_{xy} \rightarrow 0$, the consecutive occurrence from x to y is very unlikely. By letting $\mathbf{A} = \{\alpha_{xy} \exp(-\alpha_{xy})\}_{D \times D}$, we have $\mathbf{A}_e = g_i \mathbf{A}$ with $g_i = \exp(\Delta_i)$.

For better scalability, we impose a practically reasonable assumption on the transition model. *Each visual cluster of \mathbf{x}_i^l is conditionally independent of another given $\mathbf{x}_{p(i)}^l$.* That is, the transition likelihood factors over individual dimensions: $f(\mathbf{x}_i^l, t_i^l | \mathbf{x}_{p(i)}^l, t_{p(i)}^l) = \prod_{d=1}^D f(x_{i,d}^l, t_i^l | \mathbf{x}_{p(i)}^l, t_{p(i)}^l)$. Consequently, from Eq.(3), we can express the transition likelihood as Gaussian distribution: $f(x_{i,d}^l, t_i^l | \mathbf{x}_{p(i)}^l, t_{p(i)}^l) = \mathcal{N}(x_{i,d}^l; g_i \mathbf{A}_{d*} \mathbf{x}_{p(i)}^l, \sigma^2)$, where \mathbf{A}_{d*} denotes the d -th row of the matrix \mathbf{A} . Finally, the log-likelihood $\log f(\mathcal{P})$ in Eq.(2) can be written

$$\begin{aligned} \log f(\mathcal{P}) &= - \sum_{l=1}^L \sum_{i \in P^l} \sum_{d=1}^D f(x_{i,d}^l) \quad \text{where} \\ f(x_{i,d}^l) &= \left(\frac{N^l}{2} \log(2\pi\sigma^2) + \frac{1}{2\sigma^2} (x_{i,d}^l - g_i \mathbf{A}_{d*} \mathbf{x}_{p(i)}^l)^2 \right) \end{aligned} \quad (4)$$

4.3. Optimization

Our optimization problem is to discover nonzero elements of \mathbf{A}^t for any $t \in [0, T]$, by maximizing the log-likelihood of Eq.(4). For statistical tractability and scalability, we take advantage of the constraints and the assumption described in previous section.

First, one difficulty during optimization is that for a fixed t , the estimator may suffer from high variance due to the scarcity of training data (*i.e.* images occurring at time t may be too few). In order to overcome this, we take advantage of the constraint that \mathbf{A}^t varies smoothly over time; thus, we can estimate \mathbf{A}^t by re-weighting the observation data near t accordingly. Second, thanks to the conditional independence assumption per dimension of visual clusters, we

can reduce the inference of \mathbf{A}^t to a *neighborhood selection*-style optimization [14], which enables to estimate the graph by *independently* solving a set of atomic weighted lasso problem for each dimension d while guaranteeing asymptotic consistency. Hence, the optimization becomes trivially parallelizable per dimension. Such property is of particular importance in our problem possibly using millions of images with many different image descriptors. Finally, we encourage a sparse solution by penalizing nonzero elements of \mathbf{A}^t . As a result, we estimate \mathbf{A}^t by iteratively solving the following optimization D times:

$$\widehat{\mathbf{A}}_{d*}^t = \operatorname{argmin}_{\mathbf{A}_{d*}} \sum_{l=1}^L \sum_{i \in P^l} w^t(i) (x_{i,d}^l - g_i \mathbf{A}_{d*}^t \mathbf{x}_{p(i)}^l)^2 + \lambda \|\mathbf{A}_{d*}^t\| \quad (5)$$

where $w^t(i)$ is the weighting of an observation of image p_i^l in photo stream l at time t . That is, if the timestamp t_i^l of p_i^l is close to t , $w^t(i)$ is large so that the observation contributes more on the graph estimation at t . Naturally, we can define $w^t(i) = \frac{\kappa_h(t-t_i^l)}{\sum_{l=1}^L \sum_{i \in P^l} \kappa_h(t-t_i^l)}$ where $\kappa_h(u)$ is Gaussian RBF kernel with a kernel bandwidth h (*i.e.* $\kappa_h(u) = \exp(-u^2/2h^2)/\sqrt{2\pi h}$).

In Eq.(5), we include ℓ_1 -regularization where λ is a parameter that controls the sparsity of $\widehat{\mathbf{A}}_{d*}^t$. It not only avoids overfitting but also is practical because only a small number of strong story branches at each node are detected so that story links are not unnecessarily complex. Consequently, our graph inference reduces to iteratively solving a standard weighted ℓ_1 -regularized least square problem, whose global optimum can be solved by scalable techniques such as the coordinate descent [6]. In summary, the graph inference can be performed in a linear time with respect to all parameters, including the number of images and nodes. We present more details of the algorithm including the pseudocode in the supplementary material.

After solving the optimization of Eq.(5) to discover the topology of the storyline graph (*i.e.* nonzero elements of $\{\mathbf{A}^t\}$), we run the *parameter learning* (*i.e.* estimating actual associated weights) while fixing the topology of the graph. Since the structure of each graph is known and all photo streams are independent of one another, we can easily solve for MLE of $\widehat{\mathbf{A}}^t$, which is similar to that of the transition matrix of k -th Markovian chains.

5. Experiments

We evaluate the proposed approach from two technical perspectives: video summarization in section 5.1 and image summarization as storylines in section 5.2.

Flickr/YouTube dataset. Fig.3.(a)–(b) summarize our Flickr dataset of 20 outdoor recreational activity classes that consists of about 2.7M images from 35K photo streams. Some classes are re-used from the datasets of [9], and the others are newly downloaded using the same crawling

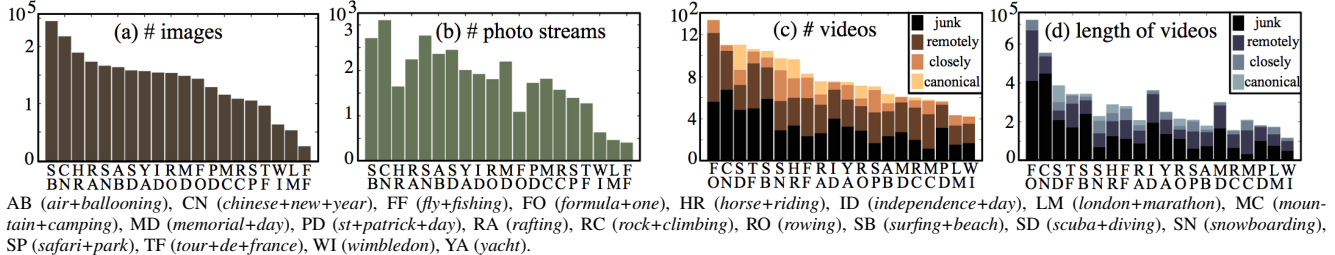


Figure 3. The Flickr/YouTube datasets of 20 outdoor recreational classes. (a)–(b) The number of images and photo streams of Flickr dataset: (2,769,504, 35,545). (c)–(d) The number and total length of YouTube videos: (15,912, 1,586.8 hours).

method, in which the topic names are used as search keywords and all queried photo streams of more than 30 images are downloaded without any filtering.

Fig.3.(c)–(d) show the statistics of our YouTube datasets with about 16K user videos. We query the same topic keywords using YouTube built-in search engines, and download only the Creative Commons licensed videos. Since YouTube user videos are extremely noisy, we manually rate them into one of four categories: *canonical*, *closely/remotely related*, and *junk*. These labels are not used by the algorithms but for the groundtruth labeling only.

5.1. Results on Video Summarization

Tasks. Due to the large-scale nature of our problems, we obtain groundtruth (GT) labels via crowdsourcing using Amazon Mechanical Turk (AMT), inspired by [8]. For each class, we randomly sample 100 test videos that are rated as *canonical* or *closely-related*, in order to use reasonably good videos rather than junk ones for algorithm evaluation. Then, we uniformly sample 50 frames from each test video, and ask at least five different turkers to select 5~10 ones that must be included when they make a storyline summary. We run our algorithm and baselines to select a small number of keyframes as a summary of each test video. We then compute the similarity-based average precision (AP) values proposed in [8], by comparing the result to the five GT summaries and then taking the mean of the APs. Finally, we compute the mean APs from all annotated test videos. We defer the detail of the AP computation to the supplementary.

Baselines. We select four baselines based on the recent video summarization studies [8, 12, 13]. The (*Unif*) uniformly samples ν keyframes from each test video. The (*KMean*) and the (*Spect*) are the two popular clustering methods, K-means and spectral clustering, respectively. They first create ν clusters and select the images closest to the cluster centers. The (*RankT*) is one of state-of-the-art keyframe extraction methods using the rank-tracing technique [1]. Our video summarization is performed in two different ways. The (*OursV*) denotes our method without involving similarity votes by images, while the (*OursIV*) is our fully-gearred method; this comparison justifies the usefulness of joint summarization between images and videos.

Results. Fig.4 reports the average precisions of our algorithms and baselines across the 20 classes. Our algorithm significantly outperforms all the baselines in most classes. For example, the mean AP of the (*OursIV*) is **0.8315**, which is notably higher than 0.8046 of the best baseline (*Spect*). The performance of the (*KMean*) and the (*Spect*) highly depends on the number of clusters ν . We change ν from 5 to 25, and report the best results.

Fig.5 compares video summarization results produced by different methods. The (*Unif*) cannot correctly handle different lengths of subshots in a single video (*i.e.* redundant images can be selected from long subshots while none from interesting short ones). One practical drawback of the (*KMean*) and the (*Spect*) is that it is hard to know the best ν beforehand even though the accuracies highly depend on ν . Overall, all algorithms except the (*OursIV*) suffer from the limitations of using low-level features only. For example, as shown in Fig.5.(a), the (*OursV*) and the (*KMean*) detect meaningless completely-gray sky frames in 3rd and 5th column, respectively. Such frames with no semantic meaning occur frequently in user videos, whereas very few in the image sets. Therefore, although (*OursIV*) uses the same low-level features, it can easily suppress such unimportant information thanks to the similarity votes by the images that photographers take more carefully with sufficient semantic intents and values².

5.2. Results on Photo Storyline Summarization

Task. It is inherently difficult to quantitatively evaluate the storyline reconstruction because there is no groundtruth available. Moreover, it is painfully overwhelming for a human labeler to evaluate the storylines summarized from large sets of images. For example, given multiple storyline graphs with hundreds of nodes created from millions of images, a human labeler may feel hopelessly devastated to judge which one is better. In order to overcome such inherent difficulty of the storyline evaluation, we design the following evaluation task via crowdsourcing.

We first run our methods and baselines to generate storyline graphs from the dataset of each class. We then sample

² Unfortunately, such semantic significance is not fully evaluated by the AP metric of Fig.4, which is solely based on low-level feature differences.

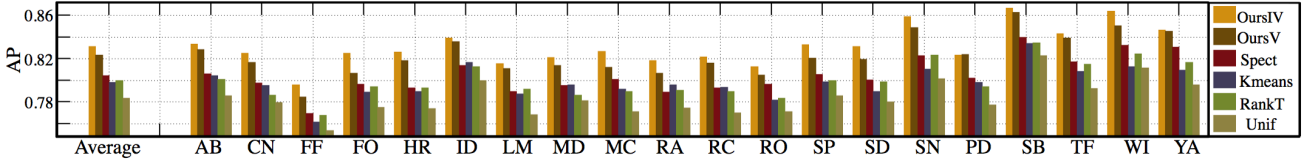


Figure 4. Comparison of mean average precisions (APs) between our methods (OursIV) and (OursV) and the baselines (Unif), (KMean), (Spect), and (RankT). The acronyms of activities are referred to Fig.3. The leftmost bar set shows the average APs for all classes. (OursIV): **0.8315**, (OursV): 0.8234, (Spect): 0.8046, (KMean): 0.7983, (RankT): 0.7997, and (Unif): 0.7837.

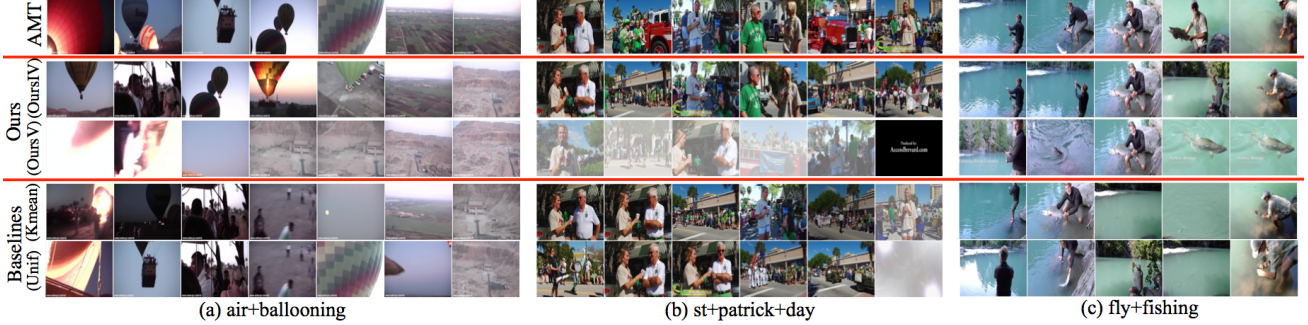


Figure 5. Qualitative comparison of video summarization results. From top to bottom, we show AMT groundtruth and the same number of selected keyframes by our algorithms (with and without similarity voting by images), and two baselines (KMean) and (Unif).

100 canonical images on the timeline as test instances \mathcal{I}_Q . Based on the storyline, each algorithm can retrieve one image that is most likely to come next after each test image $I_q \in \mathcal{I}_Q$. That is, we first identify which node corresponds to the I_q , and follow the most strongly connected edge to the next likely node, from which the central image is retrieved. For evaluation, a turker is shown the test image I_q , and then a pair of images predicted by our algorithm and one of baselines in a random order, and asked to choose the one that is more likely to follow I_q than the other. We design the AMT task as a pairwise comparison instead of a multiple-choice question (*i.e.* selecting the best one among the outputs of all algorithms), to make the annotation simple enough for any turker to instantaneously complete. We obtain such pairwise comparison for each of \mathcal{I}_Q from at least three different turkers. In summary, the underlying idea of our evaluation is that we recruit a crowd of labelers, each of who evaluates only a basic unit (*i.e.* *an important edge* of the storyline), instead of the assessment of the whole storyline, which is practically impossible.

Baselines. We compare three baselines with our approach. The (Page) is a Page-Rank based image retrieval that simply selects the top-ranked image around the timestamp of I_q . It is compared to show that storylines as sequential summary can be more useful than the traditional retrieval method. The (HMM) is an HMM based method that has been popularly applied for sequence modeling. This comparison can tell the importance of our branching structure over the linear storyline of the (HMM). The (Clust) is a simple clustering-based summarization on the timeline [9], in which images are distributed on the timeline of 24 hours, and grouped into 10 clusters at every 30 minutes. We also

compare with our algorithm using images only, denoted by (OursI), in order to quantify the improvement by joint summarization with videos. We present more details of application of our algorithm and baselines in supplementary.

Results. Fig.6 shows the results of pairwise preference tests obtained via AMT between our algorithm and each baseline. The number indicates the mean percentage of responses that choose our prediction as a more likely one to come next after each I_q than that of the baseline. That is, the number should be higher than at least 50% to validate the superiority of our algorithm. Even considering a certain degree of unavoidable noisiness of AMT labels, our output is significantly preferred by AMT annotators. For example, our algorithm (OursVI) gains 75.9% of votes, far outdistancing the best baseline (HMM). Importantly, more than two thirds of responses (*i.e.* 67.9%) prefer the results of the (OursVI) over those of the (OursI), which indeed support our argument that a crowd of videos help improve the quality of the storylines from users' point of view.

Fig.7 illustrates another interesting qualitative comparison between our method and baselines. Given a pair of images that are distant in a novel photo stream (*i.e.* images within red boundaries in Fig.7.(a)), each algorithm predicts 10 images that are likely to occur between them using its own storyline graph (*i.e.* each algorithm finds out the *best* path between the two images). As shown in Fig.7.(a), our algorithm (in the second row) can retrieve the images that are very similar to the hidden groundtruths (in the first row). Using the iterative Viterbi algorithm, the (HMM) retrieves reasonably good but highly redundant images, which are in part due to its inability to represent various branching structures. The (Page) retrieves top-ranked images (*i.e.*

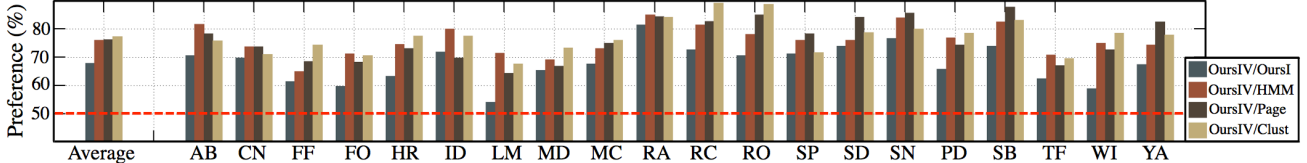


Figure 6. The results of pairwise preference tests between our method (OursIV) and each baseline via Amazon Mechanical Turk. The numbers indicates the percentage of responses that our prediction is more likely to occur next after I_q than that of the baseline. At least the number should be higher than 50% (shown in red dotted line) to validate the superiority of our algorithm. The leftmost bar set shows the average preference of our (OursIV) for all 20 classes: [67.9, 75.9, 76.1, 77.1] over (OursV), (HMM), (Page), and (Clust).

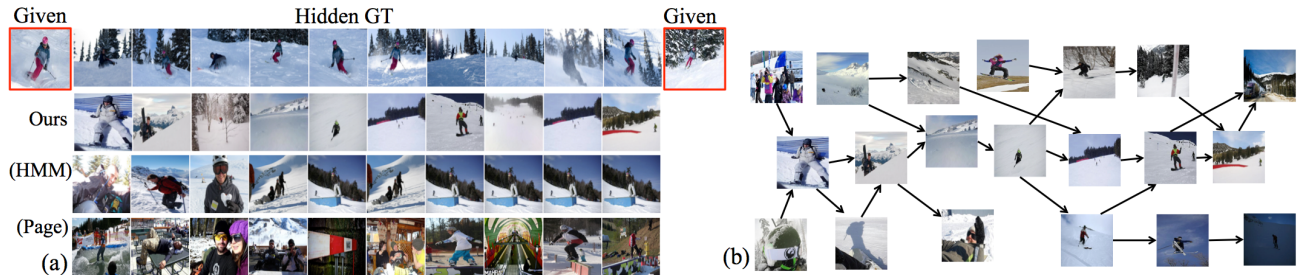


Figure 7. Examples of an qualitative comparison between our method and baselines. (a) Given a pair of distant images in a photo stream (*i.e.* the ones within red boundaries), each algorithm predicts the best path between them and samples 10 images. (b) A downsized version of our storyline graph used for the prediction of (a).

representative and high-quality images) at each query time point. However, it has no use of the sequential structure, and thus there is no connected story between retrieved images. Fig.7.(b) shows a downsized version of our storyline graph that is used for creating the result of Fig.7.(a). Although we can freely choose the temporal granularity to zoom in or out the storylines, we here show only a small part of them for better visibility. We present more illustration examples of storyline graphs in the supplementary.

6. Conclusion

In this paper, we proposed a scalable approach to jointly summarize large sets of Flickr images and YouTube videos, and created a novel structural summary as storyline graphs visualizing a variety of underlying narrative branches of topics. We validated the superior performance of our approach via the evaluation using Amazon Mechanical Turk.

References

- [1] W. Abd-Almageed. Online, Simultaneous Shot Boundary Detection and Key Frame Extraction for Sports Videos Using Rank Tracing. In *ICIP*, 2008. 6
- [2] O. Boiman, E. Shechtman, and M. Irani. In Defense of Nearest-Neighbor Based Image Classification. In *CVPR*, 2008. 3
- [3] C. Y. Chen and K. Grauman. Watching Unlabeled Video Helps Learn New Human Actions from Very Few Labeled Snapshots. In *CVPR*, 2013. 2
- [4] L. Chen, L. Duan, and D. Xu. Event Recognition in Videos by Learning from Heterogeneous Web Sources. In *CVPR*, 2013. 2
- [5] J. Deng, W. Dong, R. Socher, L. J. Li, K. Li, and L. Fei-Fei. ImageNet: A Large-Scale Hierarchical Image Database. In *CVPR*, 2009. 2
- [6] W. J. Fu. Penalized Regressions: The Bridge Versus the Lasso. *J. Computational Graphical Statistics*, 7:397–416, 1998. 5
- [7] A. Gupta, P. Srinivasan, J. Shi, and L. S. Davis. Understanding Videos, Constructing Plots: Learning a Visually Grounded Storyline Model from Annotated Videos. In *ICCV*, 2009. 2
- [8] A. Khosla, R. Hamid, C. J. Lin, and N. Sundaresan. Large-Scale Video Summarization Using Web-Image Priors. In *CVPR*, 2013. 2, 3, 6
- [9] G. Kim and E. P. Xing. Jointly Aligning and Segmenting Multiple Web Photo Streams for the Inference of Collective Photo Storylines. In *CVPR*, 2013. 2, 5, 7
- [10] G. Kim, E. P. Xing, L. Fei-Fei, and T. Kanade. Distributed Cosegmentation via Submodular Optimization on Anisotropic Diffusion. In *ICCV*, 2011. 3, 4
- [11] M. Kolar, L. Song, A. Ahmed, and E. P. Xing. Estimating Time-Varying Networks. *Ann. Appl. Stat.*, 4(1):94–123, 2010. 4
- [12] Y. J. Lee, J. Ghosh, and K. Grauman. Discovering Important People and Objects for Egocentric Video Summarization. In *CVPR*, 2012. 2, 6
- [13] Z. Lu and K. Grauman. Story-Driven Summarization for Egocentric Video. In *CVPR*, 2013. 2, 6
- [14] N. Meinshausen and P. Bühlmann. High-Dimensional Graphs and Variable Selection with the Lasso. *Ann. Statist.*, 34(3):1436–1462, 2006. 5
- [15] H. Misra, F. Hopfgartner, A. Goyal, P. Punitha, and J. M. Jose. TV News Story Segmentation Based on Semantic Coherence and Content Similarity. In *MMM*, 2010. 2
- [16] A. Prest, C. Leistner, J. Civera, C. Schmid, and V. Ferrari. Learning Object Class Detectors from Weakly Annotated Video. In *CVPR*, 2012. 2
- [17] M. G. Rodriguez, D. Balduzzi, and B. Schölkopf. Uncovering the Temporal Dynamics of Diffusion Networks. In *ICML*, 2011. 5
- [18] I. Simon, N. Snavely, and S. M. Seitz. Scene Summarization for Online Image Collections. In *ICCV*, 2007. 2
- [19] L. Song, M. Kolar, and E. Xing. Time-Varying Dynamic Bayesian Networks. In *NIPS*, 2009. 4
- [20] K. Tang, V. Ramanathan, L. Fei-Fei, and D. Koller. Shifting Weights: Adapting Object Detectors from Image to Video. In *NIPS*, 2012. 2
- [21] A. Torralba, R. Fergus, and W. T. Freeman. 80 Million Tiny Images: A Large Data Set for Nonparametric Object and Scene Recognition. *IEEE PAMI*, 30:1958–1970, 2008. 2, 3